Improved understanding of the acoustophoretic focusing of dense suspensions in a microchannel

S. Karthick and A. K. Sen*

Department of Mechanical Engineering, Indian Institute of Technology Madras, Chennai 600036, India

(Received 24 August 2017; published 21 November 2017)

We provide improved understanding of acoustophoretic focusing of a dense suspension (volume fraction $\varphi > 10\%$) in a microchannel subjected to an acoustic standing wave using a proposed theoretical model and experiments. The model is based on the theory of interacting continua and utilizes a momentum transport equation for the mixture, continuity equation, and transport equation for the solid phase. The model demonstrates the interplay between acoustic radiation and shear-induced diffusion (SID) forces that is critical in the focusing of dense suspensions. The shear-induced particle migration model of Leighton and Acrivos, coupled with the acoustic radiation force, is employed to simulate the continuum behavior of particles. In the literature, various closures for the diffusion coefficient D_φ^* are available for rigid spheres at high concentrations and nonspherical deformable particles [e.g., red blood cells (RBCs)] at low concentrations. Here we propose a closure for D_φ^* for dense suspension of RBCs and validate the proposed model with experimental data. While the available closures for D_φ^* fail to predict the acoustic focusing of a dense suspension of nonspherical deformable particles like RBCs, the predictions of the proposed model match experimental data within 15%. Both the model and experiments reveal a competition between acoustic radiation and SID forces that gives rise to an equilibrium width w^* of a focused stream of particles at some distance L_{eq}^* along the flow direction. Using different shear rates, acoustic energy densities, and particle concentrations, we show that the equilibrium width is governed by Péclet number Pe and Strouhal number St as $w^* = 1.4(\mathrm{Pe\,St})^{-0.5}$ while the length required to obtain the equilibrium-focused width depends on St as $L_{eq}^* = 3.8/(\mathrm{St})^{0.6}$. The proposed model and correlations would find significance in the design of microchannels for acoustic focusing of dense suspensions such as undiluted blood.

DOI: 10.1103/PhysRevE.96.052606

I. INTRODUCTION

Sorting and manipulation of biological suspensions in microchannels has become a potential tool in contemporary laboratory-on-a-chip (LOC) technologies and micro-total analysis systems [1–3]. Dense suspensions such as undiluted blood contain particles at high concentrations in which the interactions between particles alter the flow behavior significantly as compared to dilute suspensions. Understanding the behavior of dense suspensions (e.g., undiluted blood) in a microchannel under the influence of external forces such as acoustic force is critical for LOC technology development. Recently, many different biotechnical applications based on acoustophoresis have emerged such as blood plasma separation and isolation of circulating tumor cells from blood [4–6].

A dense suspension (volume fraction $\varphi > 10\%$) such as undiluted blood can be modeled using direct numerical simulation (DNS) and continuum modeling. The computational cost of the continuum modeling is significantly lower compared to that of DNS [7]. DNS models resolve the deformation dynamics of the particles and hydrodynamic particle-particle interaction between the particles in a fluid medium [8]. In continuum modeling, the particles are described by a continuous concentration field coupled to the continuity and Navier-Stokes equations. The interactions between the particles are imposed through the concentration gradient and other physical parameters [9]. The main objective of this work is to provide improved understanding of acoustophoretic focusing of dense suspension in a microchannel subjected to an acoustic standing wave using a proposed theoretical model and experiments.

The mixture theory or theory of interacting continua is a continuum model where blood flow is modeled as two superimposed continua, representing the plasma and red blood cells (RBCs). In a recent study, by using mixture theory, Kim *et al.* [10] simulated blood flow in a microchannel and validated the simulations using experiments. Lei *et al.* [11] showed that the continuum model descriptions are valid for $\frac{a}{D} \leqslant 0.02$, where a is the particle radius, and D is the microchannel length scale.

Ley *et al.* [12] reported continuum modeling of a dense suspension in a microchannel flow subjected to acoustophoresis and magnetophoresis. However, the model failed to capture the behavior of a dense suspension when the particle concentration is greater than 0.1, and the advection time scale in their study was in the same order as the acoustophoresis time scale. Moreover, the model does not account for the shear-induced diffusion (SID) force due to the interaction between the particles in a dense suspension, which is possibly the main reason for the failure of the model [13,14]. SID is the diffusive motion of microparticles in a shear flow [14]. Due to the hydrodynamic interactions between the neighboring particles, the distance between the particles after the interaction increases as compared to that before the interaction [15].

We consider a suspension as dense or highly concentrated if the volume fraction is more than 10%. In a flow of highly concentrated suspensions, the SID plays a major role in the migration of microparticles. The continuum model developed in this work accounts for the acoustophoretic as well as SID forces and is validated with experimental data using undiluted blood suspension. Experiments were

*Corresponding author: ashis@iitm.ac.in

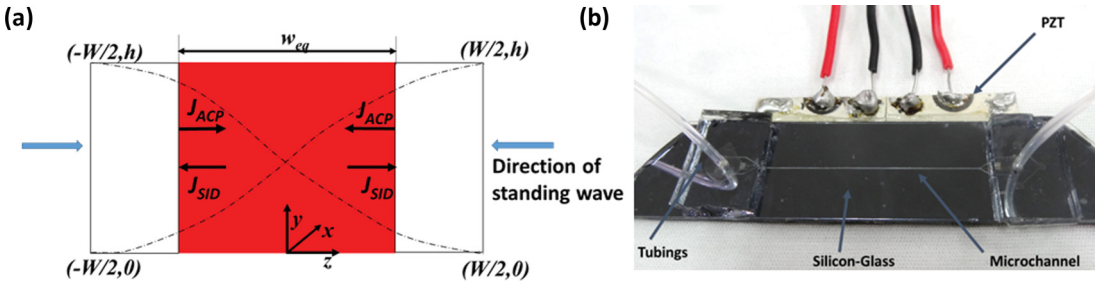

FIG. 1. (a) Schematic of the acoustophoretic focusing of a dense suspension (e.g., whole blood). (b) Photograph of an acoustophoresis chip.

performed to obtain acoustophoretic focusing of suspensions of various concentrations at various acoustic energy densities and flow rates. Our study revealed that the physics of the acoustophoretic focusing is governed by two dimensionless parameters: the Péclet number Pe (ratio of diffusion and advection time scales) and Strouhal number St (ratio of advection and acoustic timescales). The equilibrium width of the focused band correlates with the Péclet number and Strouhal number, while the length required to obtain the equilibrium-focused width correlated with the Strouhal number. The proposed correlations would find significance in the design of microchannels for acoustic-based separation of dense suspensions such as undiluted blood.

First, we provide a detailed description of the theoretical model. Next, we present the device fabrication and experimental protocols. Finally, we present and discuss the results of the continuum model and experiments. Based on the results, the equilibrium width and the length required to achieve the equilibrium width are correlated with dimensionless parameters Péclet number and Strouhal number.

II. THEORETICAL MODEL

When a dense suspension (e.g., undiluted blood) is infused into a microchannel and is subjected to an acoustic standing wave, the acoustic radiation force acting on the particles moves particles towards the center (pressure node) of the microchannel. In this process, the concentration profile becomes nonhomogeneous along the direction of the standing wave. This nonhomogenous concentration profile causes SID [13], and the particle migration due to SID tends to oppose the acoustic migration. SID is zero at the entrance of the microchannel, but due to the acoustic focusing of particles, it increases downstream. At some location along the channel, the SID force is balanced by the ACP force, thereby establishing the equilibrium-focused band width as shown in Fig. 1(a). The mixture model that is employed to simulate the focusing of the particle suspension using acoustophoresis is discussed in the following sections. Other interactions like Brownian, Van der Waals, gravity, and electrostatic are also present in the suspension [16]. However, it has been found that the order of magnitude of the above interactions is negligible as compared to SID (hydrodynamic interaction) [16]. The secondary radiation forces acting on the RBCs are also shown to be negligible compared to the primary radiation force [13].

A. Model setup

A simple two-dimensional (2D) microchannel of width W and length L is considered. The model represents the actual microchannel device, in which the width $W = 400\mu$m is along the acoustic standing wave direction and length $L = 40$ mm is along the flow direction. In the model, at the inlet of the microchannel, the velocity boundary condition is used, which is obtained by dividing the flow rate used in the experiments with the cross-sectional area of the channel (120 μm $\times$ 400 μm). Height of the channel is not considered in our model (Hele-Shaw flow analysis) for two reasons. First, there is no external force acting on the particles along the direction of the channel height, so we assume that the concentration profile does not vary in this direction. Second, generally a three-dimensional (3D) model is computationally more expensive as compared to a 2D model, and in this case 3D modeling becomes significantly time consuming since L (40 mm) $>>$ (0.4 mm). Moreover, our results show that the 2D model is able to accurately predict the experimental conditions, which is possibly because of the first reason. To proceed with the modeling, we assume the red blood cells (RBCs) to be spherical and monodisperse, but in reality RBCs are biconcave and polydispersed (volume can vary from 80 fl to 96 fl) [17]. The average radius of RBCs $= 2.8$ μm used in our model was obtained from the average volume of erythrocytes 90 fl (using complete blood count test). The local concentration of RBCs is described by the continuous field. The inlet concentration of RBCs is varied from 0.1 to 0.425. Our model is completely described by three parameters: concentration field, velocity field, and pressure field. The acoustic energy density in our model is varied from 30 J/m^3 to 90 J/m^3.

B. Mixture model

A suspension is a mixture of solid particles and a liquid. Using the theory of interacting continua (mixture theory), blood is modeled as a two-component mixture: plasma and RBCs. The plasma is assumed to behave as a Newtonian fluid, and the RBCs are modeled as a suspension of rigid spherical particles with a viscosity dependence on the shear rate and the hematocrit. The dynamics of a suspension can be modeled by the momentum transport equation for the mixture, continuity equation, and transport equation for the solid phase volume fraction. The proposed shear-induced migration model is formulated in terms of particle diffusion fluxes. The continuity equation can be written as [7,17,18]

$$(\rho_f - \rho_s)\{\nabla \cdot [\varphi(1 - c_s)\mathbf{u_s}]\} + \rho_f(\nabla \cdot \mathbf{u}) = 0, \qquad (1)$$

where ρ_f and ρ_s are the densities of fluid and solid particles respectively, c_s and $\mathbf{u_s}$ are the mass fraction and velocity of the solid particles, and φ is the volume fraction. The mixture velocity can be written in terms of the fluid and solid velocities as

$$\mathbf{u} = \frac{(1-\varphi)\rho_f\,\mathbf{u_f} + \varphi\rho_s\mathbf{u_s}}{\rho}, \tag{2}$$

where ρ is the density of the mixture given as

$$\rho = (1-\varphi)\rho_f + \varphi\rho_s. \tag{3}$$

The momentum equations reads [7,17,18]

$$\rho\frac{\partial \mathbf{u}}{\partial t} + \rho(\mathbf{u}\cdot\nabla)\mathbf{u} = \nabla\cdot\{-pI + \mu[\nabla\mathbf{u} + (\nabla\mathbf{u})^T]\} - \nabla\cdot\left\{[\rho c_s(1-c_s)]\mathbf{u_{slip}}\cdot\mathbf{u_{slip}}\right\}. \tag{4}$$

The set of equations above were solved using COMSOL Multiphysics software [18], which employs a numerical formulation based on the slip velocity $\mathbf{u_{slip}}$ between the fluid and solid phases. In the laminar flow mixture model, the slip velocity is modeled as a function of particle diffusive fluxes as

$$\mathbf{u_{slip}} = \frac{J_s}{\rho_s\varphi(1-c_s)}, \tag{5}$$

where J_s, ρ_s, and c_s are diffusive flux, density, and mass fraction of the suspended particles, respectively. In this case, the diffusion flux due to SID competes with the diffusion flux due to acoustophoresis (ACP). Thus the diffusion flux acting on the particles is the sum of the fluxes due to SID (J_{SID}) and ACP (J_{ACP}), which is expressed as

$$J_s = J_{\mathrm{SID}} + J_{\mathrm{ACP}}. \tag{6}$$

C. Modeling of shear-induced diffusion

We employ the diffusion model developed by Phillips [9] based on the scaling arguments of Leighton and Acrivos [19]. The SID flux in terms of gradients in volume fraction and shear rate can be written as [9,19–21]

$$J_{\mathrm{SID}} = D_\varphi\nabla\varphi + D_{\dot\gamma}\nabla\dot\gamma, \tag{7}$$

where D_φ and $D_{\dot\gamma}$ are the diffusion coefficients due to the gradient in volume fraction φ and shear rate$\dot\gamma$. In the literature, various models are available for D_φ and $D_{\dot\gamma}$. Diffusion coefficients can be expressed as $D_\varphi = D^*_\varphi\dot\gamma a^2$ and $D_{\dot\gamma} = D^*_{\dot\gamma}a^2$ where D^*_φ and $D^*_{\dot\gamma}$ are functions of concentration, shape, and deformability of particles suspended in the fluid [14]. D^*_φ and $D^*_{\dot\gamma}$ are well established for spherical and rigid particles at dilute and high concentrations [14]. However, since RBCs are deformable and nonspherical, D^*_φ for RBCs is very different from that of hard spherical particles [14]. Recently, Grandchamp *et al.* [14] showed that at a moderate hematocrit concentration ($\varphi = 0.15$), D^*_φ is equal to 1.7φ, for RBCs, which is nearly one order of magnitude higher as compared to $D^*_\varphi = 0.2\varphi$ for rigid and smooth spheres. The above observation is explained as follows. In a suspension of rigid particles, the interaction between any two particles does not lead to any modification of the structure of the suspension because of the linearity and reversal symmetry of the Stokes equation, and three- or more-body interactions are necessary to break the symmetry of the problem. This is the reason for negligible D^*_φ in the case of a dilute suspension where two-particle interactions are dominant and significant D^*_φ in case of a highly concentrated suspension where three- or more-body interactions are dominant.

In suspensions of deformable particles such as drops, vesicles, or cells, the deformation of objects under shear breaks the symmetry of the problem, and there is repulsion between two particles when their trajectories meet under shear flow: the cross-streamwise distance between two objects is larger after they have met each other in the shear flow [15]. This has been observed experimentally and numerically for drops and vesicles. Various closures have been developed for D^*_φ in case of rigid spheres at high concentration in a suspension. The closure for D^*_φ established by Leighton and Acrivos [19] is widely used in the literature, which is given as $D^*_\varphi = 0.33\varphi^2(1+0.5e^{8.8\varphi})$. However, a closure for D^*_φ in the case of RBCs at high concentrations is not established in literature.

We attempted various closures for D^*_φ available in literature for dilute blood cells as well as rigid spheres [9] in our model, but these closures failed to predict the actual behavior when compared with experimental results. Comparison of these failed models with experimental results is discussed in Sec. IV B. Here we propose a closure for D^*_φ that was able to accurately represent the actual phenomena in case of both dilute and undiluted blood. In the proposed closure, the low-concentration diffusion term for RBCs, i.e., $D^*_\varphi = 1.7\varphi$ is added to the high-concentration diffusion term for rigid spheres $D^*_\varphi = 0.33\varphi^2(1+0.5e^{8.8\varphi})$. So we take $D^*_\varphi = 1.7\varphi + 0.33\varphi^2(1+0.5e^{8.8\varphi})$ and $D^*_{\dot\gamma}$ is modeled as $0.42\varphi^2a^2$ [21]. The justification for this particular approach can be given as follows. At moderate concentrations ($\varphi = 0.1$–0.2), $1.7\varphi >> 0.33\varphi^2(1+0.5e^{8.8\varphi})$ and at high concentrations ($\varphi > 0.45$), $1.7\varphi << 0.33\varphi^2(1+0.5e^{8.8\varphi})$. So the addition of the two terms in the model could provide meaningful predictions in the corresponding regimes. The closure obtained by addition of the terms predicted results that match well experimental results as discussed in Sec. IV B.

Thus the diffusive flux due to SID is written as

$$J_{\mathrm{SID}} = [1.7\varphi + 0.33\varphi^2(1+0.5e^{8.8\varphi})]\dot\gamma a^2\nabla\varphi + 0.42\varphi^2a^2\nabla\dot\gamma. \tag{8}$$

The diffusion coefficients are anisotropic; the diffusion coefficients in the plane of shear is higher by approximately a factor of 1.5–2 than that in the vorticity direction [14]. To incorporate the diffusion coefficients in the shear and vorticity directions into the rectangular channel flow model, shear rate is defined as [22]

$$\dot\gamma = \frac{\left(\frac{\partial u}{\partial z}\right)^2 + 0.67\left(\frac{\partial u}{\partial y}\right)^2}{\sqrt{\left(\frac{\partial u}{\partial z}\right)^2 + \left(\frac{\partial u}{\partial y}\right)^2}}. \tag{9}$$

Here we assume that the diffusion coefficient in the plane of shear is 1.5 times higher than that in the vorticity direction ($1/1.5 = 0.67$), $\frac{\partial u}{\partial z}$ is calculated from 2D simulations, and $\frac{\partial u}{\partial y}$ is taken as $\frac{U^2_{\max}}{(H/2)^2}$ where is the channel height and is assumed to be 1.5 times of the average velocity.

D. Modeling of acoustic radiation force diffusion flux

The acoustic radiation force F_{ACP} acting on a small spherical particle subjected to acoustic standing wave, when the particle radius a is much smaller than the acoustic wavelength λ (i.e., $a << \lambda$), is governed by [23–25]

$$F_{\mathrm{ACP}} = 4\pi a^3 E_{ac} k \sin(2kz)\phi, \tag{10}$$

$\phi = \frac{\rho_p + \frac{2}{3}(\rho_p - \rho_o)}{2\rho_p + \rho_o} - \frac{1}{3}\frac{\beta_p}{\beta_o}$, $\beta_o = \frac{1}{\rho_o c_o^2}$, $\beta_p = \frac{1}{\rho_p c_p^2}$, $E_a c = \frac{P_a}{4\rho_o {c_o}^2}$, where E_{ac} is acoustic energy density, k is wave number, z is distance from the wall, ϕ is the contrast factor, ρ_p is the density of the particle, ρ_o is the density of the medium, β_p is the compressibility of the particle, β_o is compressibility of the medium, c_p is the velocity of sound in the particle, c_o is the velocity of sound in the medium, and P_a is the acoustic pressure amplitude.

The diffusive flux due to acoustic radiation force is taken as [7,12]

$$J_{\mathrm{ACP}} = f_h u_{ac} \varphi, \tag{11}$$

where f_h and u_{ac} are the hindrance function and single particle mobility, respectively. The single particle mobility u_{ac} can be obtained by equating drag force with the acoustic radiation force given in Eq. (9) as

$$u_{ac} = \frac{2a^2 E_{ac} \varnothing k \sin(2kz)}{3\eta_f}, \tag{12}$$

where η_f is viscosity of the fluid in which the particle is suspended. The viscosity of plasma (fluid medium for the RBCs) is taken as 0.0012 in our model [17]. The hindrance function f_h can be written as [21]

$$f_h = (1-\varphi)^2 \frac{\eta_f}{\eta_s}, \tag{13}$$

where is the viscosity of suspension. The viscosity of the blood suspension in our fluid dynamic model is considered to be a function of shear rate and hematocrit. The Quemada viscosity model [17,26] was used to represent this dependency as

$$\eta_s = \eta_f \left\{ 1 - \frac{\varphi}{2} \left[k_\infty - \frac{k_0 - k_\infty}{1 + \left(\frac{\dot{\gamma}}{\dot{\gamma}_c}\right)^q} \right] \right\}^{-2}. \tag{14}$$

Here the values [17] of $k_0, k_\infty, \dot{\gamma}_c$, and q are taken as $(55\varphi^{0.7} e^{-6\varphi} + 1.9)$, $[1.65(\varphi + 0.05)^{-0.3}]$, 1.0, and 0.5.

III. EXPERIMENTS

A. Device fabrication

A microchannel of dimension 120μm (height)×400μm (width)×40 mm (length) is etched in a < 100 > silicon wafer of 0.5mm thickness using deep reactive ion etching. The inlet and outlet holes (0.2 mm diameter) are drilled in the silicon wafer. The silicon wafer containing the microchannel is sealed with a planar glass slide using anodic bonding. Polyethylene tubing was used for the fluidic connection between a syringe pump (TSE Systems, Germany) and the inlet port and between the outlet port and a waste reservoir. The standing acoustic wave in the microchannel was established by applying an RF signal to the lead zirconate titanate (transducer (Sparkler Ceramics, India) attached to the bottom of the silicon substrate using epoxy glue. A photograph of the assembled acoustic chip is shown in Fig. 1(b). The RF signal was generated using a function generator (SMB100A, Rohde & Schwarz, Germany) and an amplifier (75A100A, Amplifier Research, USA). The operating frequency was approximately 1.80 MHz, and the power input ranged from 300 mW to 1.0 W. At different input power, the acoustic energy densities in the microchannel were measured using a particle-tracking method [24]. Sample blood at different hematocrit concentrations in the range 10%–42.5% was infused into the microchannel at different flow rates in the range 5–50μl/min. The width of the focused band of RBCs at different locations along the microchannel was captured using a CCD camera (Edge, Dino-lite, Taiwan). From the experimental measurements, the equilibrium-focused band and the length of the microchannel required to attain the equilibrium-focused band were obtained.

B. Measuring acoustic property of polystyrene beads

As mentioned in Sec. III A, the acoustic energy densities in the microchannel can be measured at different input power using the particle-tracking method [24]. However, to measure the acoustic energy density, the acoustic properties of the microparticles including density and the speed of sound must be known. In our work, polystyrene beads (Invitrogen, Thermo Fisher Scientific, USA) of 10 μm diameter and density $\rho_p = 1050$ kg/m^3 (available in the manufacturer's data sheet) were used. However, the speed of sound in polystyrene beads had to be determined to evaluate acoustic energy density in a continuous medium. In the literature, various values for the speed of sound in polystyrene beads in the range 1700–2400 m/s have been reported [25,27,28]. So we had to precisely determine the speed of sound in the polystyrene beads we used from our own experiments, which was later utilized to accurately predict the energy density.

The speed of sound in polystyrene beads can be determined by matching the acoustic impedance of the beads with that of the continuous medium in which the beads are suspended, i.e., by making acoustic contrast factor (ϕ) of the beads with respect to the continuous medium equal to zero [29]. So from Eq. (10), we have

$$\frac{\rho_p + \frac{2}{3}(\rho_p - \rho_o)}{2\rho_p + \rho_o} - \frac{1}{3}\frac{\rho_o c_o^2}{\rho_p c_p^2} = 0. \tag{15}$$

In Eq. (15), all other terms except the speed of sound in the polystyrene beads are known, which can be determined. To match the acoustic impedance of polystyrene beads with that of the continuous medium, the beads were suspended in iodixanol solution (Opti-Perp, Sigma-Aldrich, USA) with varying concentration of iodixanol mixed with DI water. The bead suspension was infused into the microchannel device and was subjected to standing acoustic waves. The migration of beads towards the pressure node was observed for all iodixanol concentrations less than 52%.

The migration of the beads towards the pressure nodes indicated that the beads exhibited positive acoustic contrast factor with respect to the continuous medium, i.e., iodixanol of concentration less than 52%. It was observed that the migration velocity of the beads towards the pressure node

decreases with the increase in the iodixanol concentration in the range 0%–52%. For 54% iodixanol concentration, there was no significant migration of beads observed. Further, with 56% iodixanol concentration, the beads migrated towards the pressure antinode, indicating that the beads exhibited negative contrast factor with respect to the continuous medium. So it was concluded that the polystyrene beads used in our experiments exhibited zero acoustic contrast factor when suspended in 54% iodixanol solution. The acoustic properties of various concentration of iodixanol solutions were recently reported by Augustsson *et al.* [29]. The properties of 54% iodixanol solution are given as $\rho_o = 1288$ kg/m^3 and $c_o = 1498$ kg/m^3. By substituting the density of polystyrene beads, we obtain the speed of sound in the polystyrene beads used in our experiments to be 1789 ± 20 m/s.

C. Measuring acoustic energy density

The acoustic energy densities in the microchannel were measured at different input powers using the particle-tracking method. Polystyrene beads (10 μm diameter) were suspended in DI water and infused into the microchannel and subjected to standing acoustic waves. The positions of particles were tracked frame by frame from video captured using a color CCD camera (Edge). By equating the acoustic radiation force given in Eq. (10) with drag force acting on the particles, the expression for the acoustic energy density is obtained as [24]

$$E_{ac} = \frac{3\mu}{4\phi t(ka)^2} \ln\left\{\frac{\tan[kz(t)]}{\tan[kz(0)]}\right\}. \tag{16}$$

In the above equation, on substituting the position of polystyrene particles at different times $z(t)$ obtained from experiments, the properties of the polystyrene beads, and the properties of the aqueous solution, the average values of E_{ac} at 300 mW and 1.0 W were found to be 40.6 ± 3.1 J/m^3 and 81.2 ± 4.9 J/m^3, respectively. The average and standard deviation values of E_{ac} were obtained by tracking 20 different beads in the channel.

IV. RESULTS AND DISCUSSION

Experiments and numerical simulations were performed to demonstrate acoustophoretic focusing of blood sample. For $E_{ac} = 80$ J/m^3, $\varphi = 0.425$, and $Q = 10$ μl/min, the width of the focused band at different locations along the flow direction obtained from experiments and simulations is depicted in Fig. 2. It is observed that the RBCs get focused towards the center of the channel (i.e., node), and the width of the focused band gradually decreases downstream. The width of the focused band at $x = 5$ mm and $x = 10$ mm is, respectively, $385 \pm 3\tilde{}\mu$m and $320 \pm 3\tilde{}\mu$m. The width of the focused band does not change further downstream beyond $x = 20$ mm, which is known as the equilibrium-focused width w_{eq}. For $x < 20$ mm, the acoustic force is higher than the SID force, thus the RBCs continue to come towards the center of the channel, and thus the width of the focused stream evolves dynamically. For $x \geqslant 20$ mm, due to higher concentration of the focused band, the ACP force is balanced by the SID force, thus giving rise to an equilibrium width that remains unchanged downstream. The equilibrium-focused width obtained from experiments and simulations was found to be, respectively, $290 \pm 3\tilde{}\mu$m and $280 \pm 3\tilde{}\mu$m. The simulation results match experimental data within 15%, which suggests that the assumptions made in the model are reasonable. The simulation results match experimental data within 15%, which validates the theoretical model. The difference between the simulation results and experimental data can be attributed to the assumption in the model that the RBCs are spherical and monodisperse.

We performed experiments and simulations to study acoustophoretic focusing of blood samples at various concentrations, acoustic energy densities, and flow rates. Based on the results, the equilibrium width of the focused band w_{eq} and the channel length required to obtain the equilibrium-focused width L_{eq} were correlated with dimensionless parameters (Péclet number Pe and Strouhal number St) that are discussed below.

A. Dimensionless numbers

The physics of the system can be characterized using the acoustophoretic time scale$\tau_{\text{ACP}} = \frac{W}{2\overline{u}_{ac}}$, SID time scale $\tau_{\text{SID}} = \frac{W^2}{8D_0}$, and advection time scale $\tau_{\text{adv}} = \frac{W}{2u_0}$, where W is the channel width, and $\overline{u}_{ac}$ is average acoustic migration velocity obtained by integrating the expression for acoustic migration velocity given in Eq. (12) from 0 to $\frac{W}{2}$, which is given as $\overline{u}_{ac} = 4a^2E_{ac}\gamma/3W\eta_f$. So the acoustophoretic time scale $\tau_{\text{ACP}} = \frac{3W^2}{8\phi a^2 E_{ac}}$. For the SID time scale, we take the diffusion coefficient $D_0 = 1.7\varphi_{in}\dot{\gamma}_{\text{avg}}a^2$, where φ_{in} is the hematocrit concentration at the inlet of the microchannel and $\dot{\gamma}_{\text{avg}}$is the average shear rate, which can be expressed as $\dot{\gamma}_{\text{avg}} = \sqrt{\frac{U_{\max}^2}{(H/2)^2} + \frac{U_{\max}^2}{(W/2)^2}}$, where H is the channel height and $U_{\max}$ is the maximum velocity at the center of the channel, and So$\tau_{\text{SID}} = \frac{W^2}{13.6\varphi_{in}\dot{\gamma}_{\text{avg}}a^2}$. In the advection time scale, u_0 is the (pluglike) fluid velocity at the channel inlet.

The dynamics of the problem can be described by the ratio of these three different time scales. The ratio of diffusion time scale τ_{SID} relative to advection time scale τ_{adv} is characterized by the Péclet number Pe. Similarly, the ratio of advection time scale τ_{adv} relative to acoustic time scale τ_{ACP} is characterized by the transient Strouhal number St as

$$\text{Pe} = \frac{\tau_{\text{SID}}}{\tau_{\text{adv}}}, \quad \text{St} = \frac{\tau_{\text{adv}}}{\tau_{\text{ACP}}}. \tag{17}$$

It is known that the larger is the time scale, the lesser is the effect. A higher Pe corresponds to the decreasing effect of SID compare to advection, and similarly, a higher St corresponds to the decreasing effect of ACP compare to advection. For a fixed advection time scale τ_{adv}, Pe is decreased by increasing the concentration of the particles φ_{in} and St is decreased by increasing the acoustic energy density E_{ac}.

The dimensionless numbers (Pe and St) govern the equilibrium-focused width w_{eq} and microchannel length required to attain the equilibrium-focused width L_{eq}, which are discussed in Secs. IV B and IV C, respectively.

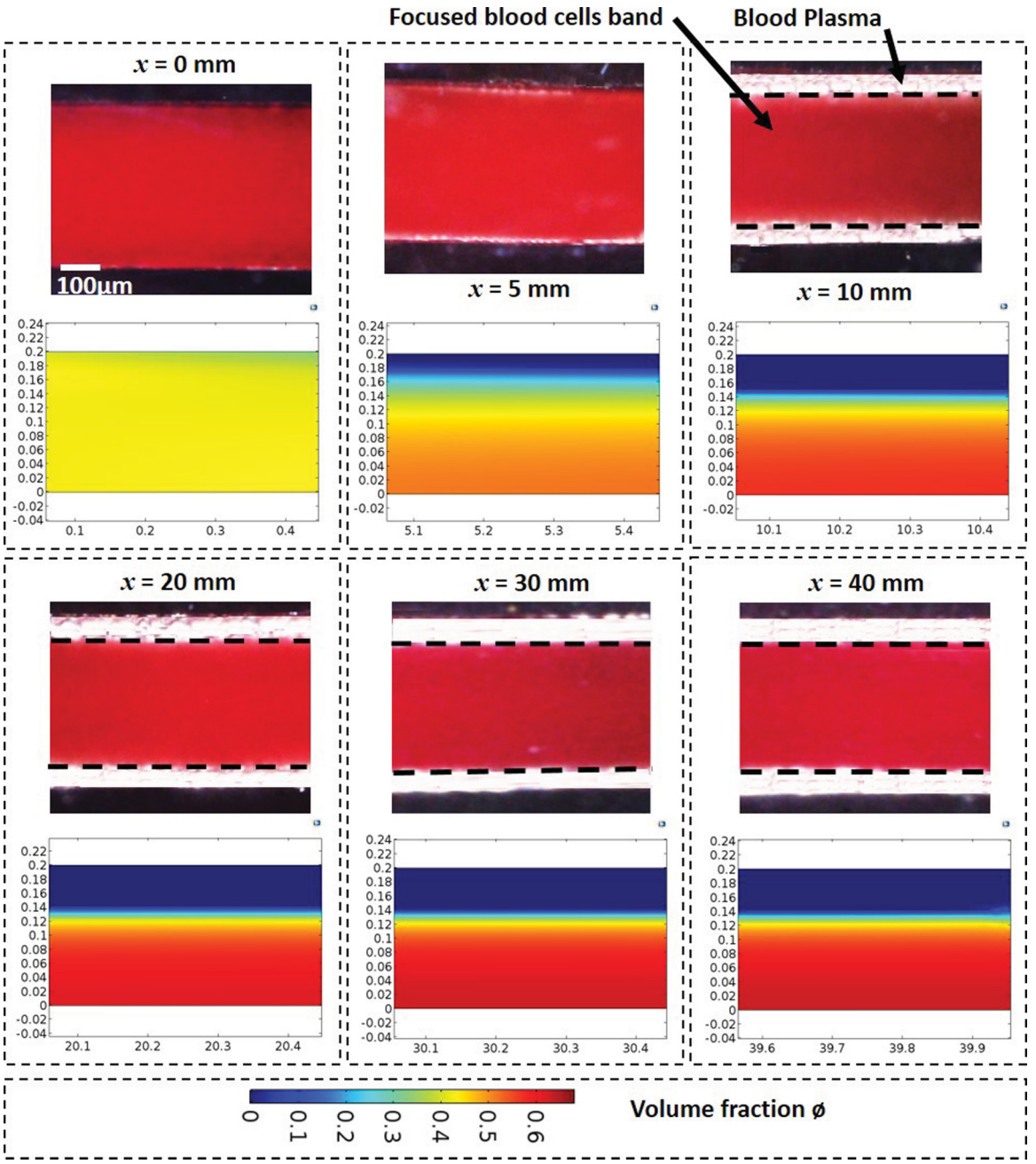

FIG. 2. The width of the focused band at different locations along the flow direction obtained from experiments and simulations for $E_{ac} = 81.2$ J/m^3, $\varphi = 0.425$, and $Q = 10$ μl/min; the simulation contours are shown for half of the channel width due to symmetry about the channel center line. At each location x, the simulation contours are shown below the experimental images. From experimental images the width of the focused band was obtained using image analysis.

B. Width of the equilibrium-focused band

We attempted different closures for D_φ^* in predicting the width of the equilibrium-focused band. The various closures are $D_f^* = [0.33\varphi^2(1 + 0.5e^{8.8\varphi})]$ proposed by Leighton *et al.* [19], $D_\varphi^* = [0.42\varphi + 1.2\varphi^2(1 - \varphi/\varphi_{\max})^{-1}]$ proposed by Phillips *et al.* [9], and $D_f^* = 1.7\varphi$ (low and medium concentration closure for RBCs) proposed by Grandchamp *et al.* [22]. We compared the results obtained using the above closures for D_φ^* with that obtained by the closure $D_\varphi^* = [1.7\varphi + 0.33\varphi^2(1 + 0.5e^{8.8\varphi})]$ proposed in this work. The comparison of results for equilibrium-focused width w_{eq} obtained using the various models with that from experiments is shown in Fig. 3. As observed, compared to the other available closures, the closure proposed in this work agrees very well with experiments (within 15%). Also, from Fig. 3, it is seen that only when the concentration of the suspension decreases ($\varphi = 0.215$) does the closure proposed by Grandchamp *et al.* approach the experimental results, as expected.

As discussed, the RBCs subjected to acoustophoretic force migrate towards the center of the channel (node) and the SID force opposes the migration. When the ACP and SID

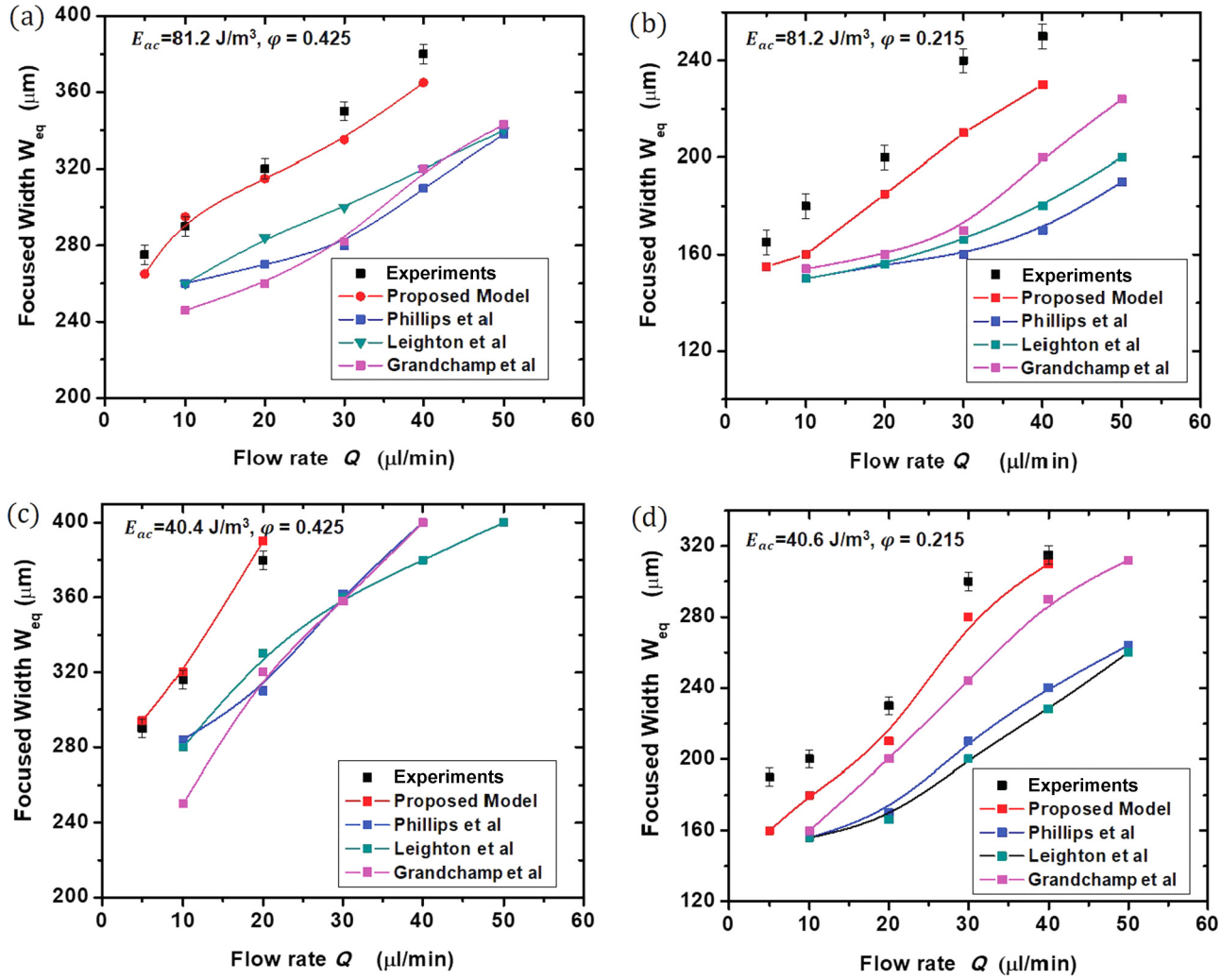

FIG. 3. Comparison of the equilibrium width of the focused band predicted using the different available models and the proposed model with that obtained from our experiments: (a) $E_{ac} = 81.2\ \mathrm{J/m^3}$, $\varphi = 0.425$; (b) $E_{ac} = 81.2\ \mathrm{J/m^3}$, $\varphi = 0.215$; (c) $E_{ac} = 40.6\ \mathrm{J/m^3}$, $\varphi = 0.425$; (d) $E_{ac} = 40.6\ \mathrm{J/m^3}$, $\varphi = 0.425$.

forces balance each other, the equilibrium-focused width is attained. Figure 4 illustrates the fundamental difference

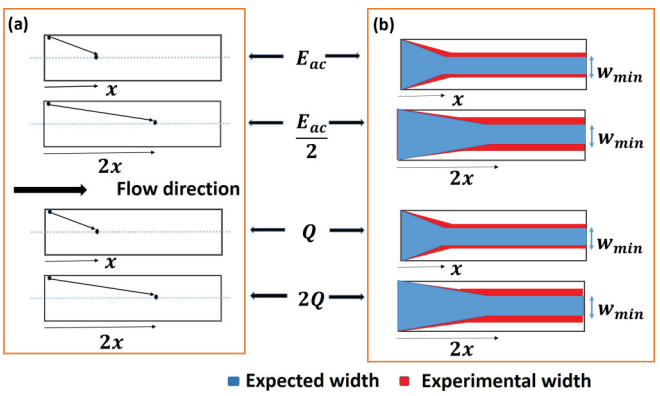

FIG. 4. Illustration of the fundamental difference between the acoustic focusing of microparticles in dilute and dense suspensions with and without the consideration of SID force. (a) Behavior of dilute suspensions; (b) behaviour of dense suspensions.

between the acoustic focusing of microparticles in dilute and dense suspensions. In dilute suspensions, focused width w_{eq} tends to zero. In a dense suspension, we might expect w_{eq} to approach w_{min}, which is the minimum possible focused width when particles are packed to maximum concentration (with maximum possible packing density). However, practically, the SID in the suspension never allows the focused width w_{eq} to attain w_{min}. Moreover, the equilibrium width of the focused band w_{eq} varies with flow rate Q and acoustic energy density E_{ac}. We observed that at a fixed flow rate Q, the equilibrium width of the focused band w_{eq} increases with a decrease in the acoustic energy density E_{ac}. Similarly, at a fixed energy density E_{ac}, the equilibrium width of the focused band w_{eq} decreases with a reduction in the flow rate Q.

The above experimental observations are explained as follows. SID is proportional to mainly the concentration gradient $\nabla\varphi$, local concentration φ, shear rate $\dot{\gamma}$, and gradient of shear rate $\nabla\dot{\gamma}$, as given by Eq. (8). A decrease in the acoustic energy density E_{ac} reduces the acoustic effect; thus to balance ACP, SID has to decrease by reducing the local concentration φ and concentration gradient $\nabla\varphi$. A reduction in the local

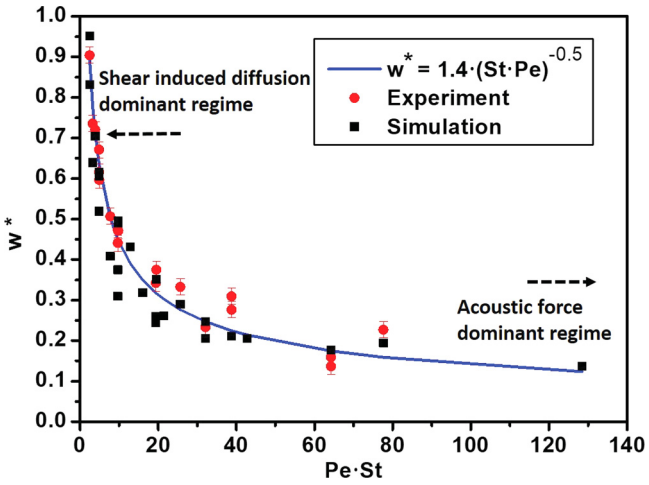

FIG. 5. The results obtained from our experiments and numerical simulations are plotted with the product of the Péclet number and the Strouhal number (Pe St), i.e., the ratio of the SID and ACP time scales, for various acoustic energy density, flow rate, and volume fraction. E_{ac} is varied from 40.6 to 81.2 J/m^3, Flow rate Q is varied from 5 μl/min to 50 μl/min, and inlet hematocrit concentration φ is varied from 10% to 42.5%.

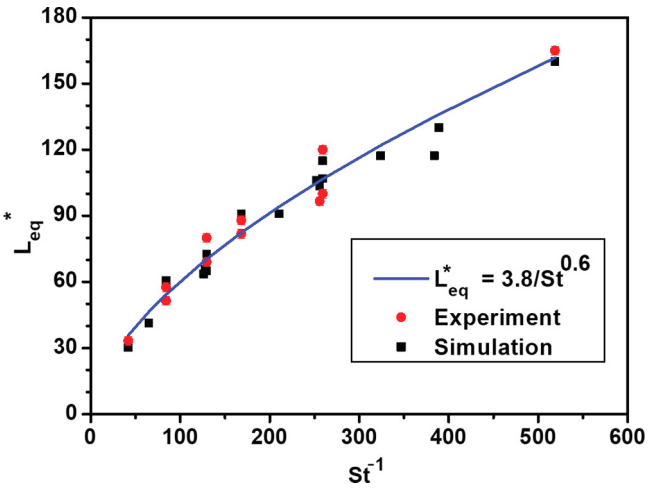

FIG. 6. The results obtained from our experiments and numerical simulations are plotted with the Strouhal number, i.e., the ratio of the ACP and advection time scales, for various acoustic energy density, flow rate, and volume fraction. E_{ac} is varied from 40.6 to 81.2 J/m^3. Flow rate Q is varied from 5 μl/min to 50 μl/min, and inlet hematocrit concentration φ is varied from 10% to 42.5%.

concentration φ and concentration gradient $\nabla\varphi$ automatically increases the equilibrium width of the focused stream $w_{\rm eq}$. An increase in flow rate Q gives rise to a higher shear rate $\dot{\gamma}$; thus to maintain the balance between SID and ACP, the local concentration φ and concentration gradient $\nabla\varphi$ has to reduce proportionally to the increase in shear rate $\dot{\gamma}$. A reduction in the local concentration φ and concentration gradient $\nabla\varphi$ automatically gives rise to a highe r$w_{\rm eq}$

We define the dimensionless equilibrium width of the focused band $w^* = \frac{w_{\rm eq}-w_{\rm min}}{W-w_{\rm min}}$ for scaling arguments. Here $w_{\rm min}$ is the minimum theoretically possible width (at maximum packing density) which can be obtained using volume conservation as follows: $U_{\rm max}w_{\rm min}\varphi_{\rm max}= U_{av}W\varphi_{\rm avg}$, $U_{\rm max}$ is the maximum velocity, and $\varphi_{\rm max}$ is the maximum random volume fraction and it is taken [30] as 0.68, U_{av} is the average velocity (which is same as the inlet velocity), and $\varphi_{\rm avg}$ is the average particle concentration (which is the same as the particle concentration at the inlet φ_{in}). Here $U_{\rm max}$ is taken as 1.5 times U_{av}. The dimensionless equilibrium width of the focused band w^* is governed by the ratio of the SID and ACP time scales.

For various acoustic energy density E_{ac}, flow rate Q, and volume fraction φ, the w^*obtained from our experiments and numerical simulations are plotted with the product of Pe and St (Pe St), i.e., the ratio of the SID and ACP time scales, in Fig. 5. The experimental data and the simulation results match well within a maximum error of 15%. Interestingly, all the data points from the experiments and simulations follow a single curve, indicating that the irrespective of the experimental conditions, w^* is related to Pe and St. Using curve fitting (for experimental data), the following relationship for w^* versus (Pe St) is obtained with a regression coefficient of 0.96:

$$w^* = 1.4(\mathrm{Pe\,St})^{-0.5}. \qquad (18)$$

Since Pe St represents the ratio of SID to ACP time scales, Pe St $>>$ 1 means the acoustic effect is more dominant as compared to the SID effect, and similarly, Pe St $<<$ 1 indicates that SID is more dominant as compared to ACP. When Pe St $>>$ 1, w^* tends to zero, which represents that the equilibrium-focused width $w_{\rm eq}$ approaches $w_{\rm min}$. On the other hand, when Pe St $\approx$ 1 or $<$ 1, this results in $w^* > 1$, which indicates that there is no focused band existing. This clearly shows that there is a critical acoustic energy density E_{ac} for given concentration φ and shear rate $\dot{\gamma}$ below which the acoustic focusing is prevented. Equation (18) enables determination of the equilibrium width of the focused band under a given experimental condition, which would have significant practical relevance in a range of LOC applications including blood plasma separation, particle and cell sorting, and microflow cytometry.

C. Length required to attain the equilibrium-focused band

As discussed, under the influence of an acoustic field, the microparticles migrate towards the center due to the ACP force which is opposed by the SID force. At some location along the channel, the SID force balances the ACP force and the equilibrium-focused width is attained. The variation in the dimensionless length required to attain the equilibrium-focused band is expressed as $L^*_{\rm eq} = L_{\rm eq}/w_{\rm min}$. For various acoustic energy density E_{ac}, flow rate Q, and volume fraction φ, the $L^*_{\rm eq}$ obtained from our experiments and numerical simulations are plotted with St, i.e., the ratio of the ACP and advection time scales, in Fig. 6. The experimental data and the simulation results match well within a maximum error of 15%. Interestingly, all the data points from the experiments and simulations follow a single curve, indicating that the irrespective of the experimental conditions $L^*_{\rm eq}$ is related to St. Using curve fitting (for experimental data), the following relationship for $L^*_{\rm eq}$ versus St is obtained with a regression

coefficient of 0.96:

$$L^*_{\rm eq} = 3.8/({\rm St})^{0.6}. \quad (19)$$

It is observed that when St << 1 (effect of acoustophoresis is negligible compared to advection), $L^*_{\rm eq}$ approaches ∞ ($L_{\rm eq} >> W$); when St $\approx$ 1 (effect of acoustophoresis is in the same order of advection), $L^*_{\rm eq}$ approaches 1 ($L_{\rm eq} = W$); when St >> 1 (effect of advection is negligible compared to the acoustophoresis) $L^*_{\rm eq}$ approaches 0 ($L_{\rm eq} << W$). The disagreement between model and experiment is within 15%, which may be due to assumptions like RBCs are monodisperse and spherical used in acoustic force modeling.

V. CONCLUSIONS

In this work we reported improved understanding of acoustophoretic focusing of a dense suspension in a microchannel subjected to an acoustic standing wave using a proposed theoretical model and experiments. The model is based on the mixture theory and employs the momentum transport equation for the mixture, continuity equation, and transport equation for the solid phase volume fraction. The model demonstrated the interplay between acoustic radiation force and shear-induced diffusion (SID) force, which is critical in the acoustophoretic focusing of dense suspensions such as undiluted blood. The SID model developed by Phillips based on the scaling arguments of Leighton and Acrivos was employed to simulate the continuum behavior of particles. In the literature, various closures for the diffusion coefficient D^*_φ are available for rigid spheres at high concentrations and deformable particles (e.g., RBCs) at low concentrations. We attempted different closures for D^*_φ proposed by Leighton *et al.* [19], Phillips *et al.* [9], and Grandchamp *et al.* [22] and compared the results with that obtained using the closure $D^*_\varphi = [1.7\varphi + 0.33\varphi^2(1 + 0.5e^{8.8\varphi})]$ proposed in this work. Modeling and simulations were performed at various acoustic energy density $E_{ac} = 40.6$ and 81.2 J/m^3 and volume fraction $\varphi = 0.215$ and 0.425. While the available closures for D^*_φ failed to predict the acoustic focusing of a dense suspension of deformable particles, the predictions of the proposed model match experimental data within 15%. The interplay of the acoustic focusing of dilute and dense suspensions with and without consideration of the SID force was explained to highlight the importance of the SID force in acoustic focusing of a dense suspension. Both the model and experiments revealed that there is a competition between acoustic radiation and SID forces that determines equilibrium width w^* of a focused stream of particles at some location $L^*_{\rm eq}$ along the flow direction. Using different shear rates $\dot\gamma$, acoustic energy densities E_{ac}, and particle concentrations φ, we show that the equilibrium width is governed by Péclet number Pe and Strouhal number St as $w^* = 1.4({\rm Pe\,St})^{-0.5}$ while the length required to obtain the equilibrium-focused width depends on St as $L^*_{\rm eq} = 3.8/({\rm St})^{0.6}$. The proposed model is computationally much less intensive as compared to other computational models such as complex direct numerical simulation models; the entire simulations reported in this work can be performed in less than a day on an ordinary personal computer. The proposed model and correlations would find significance in the design of microchannels for acoustic focusing of dense suspensions such as undiluted blood.

ACKNOWLEDGMENTS

This work was supported by the Ministry of Human Resources and Development (MHRD) (IMPRINT) India via Grant No. 35-16/2016TS/I, IIT/SRIC/ME/GDD/2016-17/242, Science & Engineering Research Board (SERB), DST India via Grant No. EMR/2014/001151, and IIT Madras via Project No. MEE1516843RFTPASHS. The authors acknowledge the CNNP, IIT Madras for supporting the device fabrication.

[1] D. R. Gossett, W. M. Weaver, A. J. Mach, S. C. Hur, H. T. K. Tse, W. Lee, H. Amini, and D. Di Carlo, Anal. Bioanal. Chem. **397**, 3249 (2010).
[2] Y. Chen, P. Li, P.-H. Huang, Y. Xie, J. D. Mai, L. Wang, N.-T. Nguyen, and T. J. Huang, Lab Chip **14**, 626 (2014).
[3] P. Sajeesh and A. K. Sen, Microfluidics Nanofluidics **17**, 1 (2014).
[4] A. Lenshof, C. Magnusson, and T. Laurell, Lab Chip **12**, 1210 (2012).
[5] M. Antfolk, S. H. Kim, S. Koizumi, T. Fujii, and T. Laurell, Sci. Rep. **7**, 46507 (2017).
[6] A. Lenshof, A. Ahmad-Tajudin, K. Jarås, A.-M. Sward-Nilsson, L. Åberg, G. Marko-Varga, J. Malm, H. Lilja, and T. Laurell, Anal. Chem. **81**, 6030 (2009).
[7] R. Rao, L. Mondy, A. Sun, and S. Altobelli, Int. J. Num. Methods Fluids **39**, 465 (2002).
[8] J. R. Clausen, D. A. Reasor, and C. K. Aidun, Comput. Phys. Commun. **181**, 1013 (2010).
[9] R. J. Phillips, R. C. Armstrong, R. A. Brown, A. L. Graham, and J. R. Abbott, Phys. Fluids A **4**, 30 (1992).
[10] J. Kim, J. F. Antaki, and M. Massoudi, J. Comput. Appl. Math. **292**, 174 (2016).
[11] H. Lei, D. A. Fedosov, B. Caswell, and G. E. Karniadakis, J. Fluid Mech. **722**, 214 (2013).
[12] M. W. Ley and H. Bruus, Lab Chip **16**, 1178 (2016).
[13] S. Karthick and A. Sen, Appl. Phys. Lett. **109**, 014101 (2016).
[14] R. Rusconi and H. A. Stone, Phys. Rev. Lett. **101**, 254502 (2008).
[15] T. Podgorski, N. Callens, C. Minetti, G. Coupier, F. Dubois, and C. Misbah, Microgravity Sci. Tech. **23**, 263 (2011).
[16] T. Dbouk, Rheology of concentrated suspensions and shear-induced migration, Ph.D. thesis, Laboratoire de physique de la matière condensée, 2011.
[17] J. Biasetti, P. G. Spazzini, U. Hedin, and T. C. Gasser, J. R. Soc. Interf. **11**, 20140403 (2014).
[18] COMSOL Multiphysics software v. 5.0 (2014).
[19] D. Leighton and A. Acrivos, Chem. Eng. Sci. **41**, 1377 (1986).
[20] D. Leighton and A. Acrivos, J. Fluid Mech. **177**, 109 (1987).
[21] H. Vollebregt, R. Van Der Sman, and R. Boom, Soft Matter **6**, 6052 (2010).

[22] X. Grandchamp, G. Coupier, A. Srivastav, C. Minetti, and T. Podgorski, Phys. Rev. Lett. **110**, 108101 (2013).
[23] L. V. King, Proc. R. Soc. London A **147**, 212 (1934).
[24] H. Bruus, Lab Chip **12**, 1014 (2012).
[25] A. Lenshof, M. Evander, T. Laurell, and J. Nilsson, Lab Chip **12**, 684 (2012).
[26] D. Quemada, P. Flaud, and P. Jezequel, Chem. Eng. Comm. **32**, 61 (1985).
[27] P. Li, Z. Mao, Z. Peng, L. Zhou, Y. Chen, P.-H. Huang, C. I. Truica, J. J. Drabick, W. S. El-Deiry, M. Dao *et al.*, Proc. Natl. Acad. Sci. USA **112**, 4970 (2015).
[28] D. Hartono, Y. Liu, P. L. Tan, X. Y. S. Then, L.-Y. L. Yung, and K.-M. Lim, Lab Chip **11**, 4072 (2011).
[29] P. Augustsson, J. T. Karlsen, H.-W. Su, H. Bruus, and J. Voldman, Nat. Comm. **7**, 11556 (2016).
[30] R. Pal, J. Biomech. **36**, 981 (2003).